2020-10-01

Mathematical modelling of concrete carbonation with moving boundary

Li, L-Y

10.1016/j.icheatmasstransfer.2020.104809
International Communication of Heat and Mass Transfer
Elsevier BV

International Communication of Heat and Mass Transfer
Accepted 08/08/2020
https://doi.org/10.1016/j.icheatmasstransfer.2020.104809

Mathematical modelling of concrete carbonation with moving boundary

Dawang Li [a], Long-yuan Li [b], Xianfeng Wang [a,*]

[a] *Guangdong Provincial Key Laboratory of Durability for Marine Civil Engineering, Shenzhen University, Shenzhen 518060, PR China*

[b] *School of Engineering, University of Plymouth, Plymouth PL4 8AA, UK*

ABSTRACT

This paper presents the mathematical models describing the diffusion of carbon-dioxide in concrete with considering the effect of concrete carbonation. The effect of concrete carbonation on carbon-dioxide diffusion is modelled by using a sink term added in the diffusion equation. It is shown that, when the carbonation reaction is much faster than the diffusion process, the diffusion of carbon-dioxide in carbonated concrete can be treated as the diffusion problem with a moving boundary, representing the diffusion front or the carbonation depth. An analytical solution is also derived for the diffusion problem with moving boundary.

Keywords: Modelling; carbon-dioxide; diffusion; concrete carbonation; moving boundary.

* Corresponding author.
E-mail address: xfw@szu.edu.cn (X.F. Wang)

1. Introduction

The corrosion of steel in reinforced concrete structures is the major concern of infrastructure owners and operators. Two major causes that are connected to corrosion of reinforcing steel in concrete structures are the carbonation and chloride attack. Carbonation is a set of reactions between atmospheric carbon-dioxide and alkaline components of concrete, producing a carbonated surface layer in which the pore solution pH value is depressed to near-neutral levels [1,2,3]. A secondary effect of carbonation, also significant in terms of its influence on reinforcing steel corrosion, is that it can cause the release of bound chloride ions into the pore solution phase of concrete that contains a modest level of chloride salts as a contaminant, thus exacerbating the corrosive nature of the electrolyte [4,5]. The carbon-dioxide diffusion has been investigated in capillaries and in a cavity with N_2-CO_2 mixture [6,7]. A variable–density single-phase incompressible model has been developed for numerical simulation of the DDC (dissolution–diffusion–convection) process of carbon-dioxide [8]. In addition, carbonation can also influence the diffusion of chloride ions in concrete as it can alter the pore volume and pore structure and thus the transport properties of concrete [9,10,11]. In certain cases the permeability of carbonated concrete may increase, as in the case of concrete made with blended cements such as blast furnace slag and fly ash concrete [9,10]; in others, it may decrease as in ordinary Portland cement concrete [4,11]. In urban and industrial areas,

where environmental pollution results in a significant concentration of carbon-dioxide, carbonation-initiated reinforcement corrosion prevails [12]. While in highways and marine or coastal structures, chloride ions, originating from deicing salts or seawater, are transported through the concrete pore network and micro-cracks and depassivate the oxide film covering the reinforcing steel and thus induce the corrosion of reinforcing steel [13]. The worst situation is when a concrete structure is subjected to both carbonation and chloride attack [14]. A recent study [15] reported that the probability of the corrosion initiation for the combined action of carbonation and chloride attack is almost two times higher than the case in which the two attacks are considered separately. This illustrates the difficulty that arises when the presence of more than one corrosion-inducing agent contributes to aggressiveness of the exposure conditions for a particular structure.

Extensive research work has been carried to understand how carbon-dioxide transports in concrete pore medium and how it reacts with cement products in concrete. Saetta et al. [16] presented a two-dimensional finite element model for the illustration of concrete carbonation mechanism. The model was used to analyse the effects of multi-dimensional moisture, heat and carbon-dioxide transport through concrete on the corrosion of a reinforcing bar placed at the corner of a concrete structure. Steffens et al. [17] developed a theoretical model to predict the carbonation of concrete structures. The model described the movement and retention of heat, moisture and carbon-dioxide by means of balance equations and diffusion laws. The governing equations of the model were solved numerically using finite element techniques. Liang and Lin [18] presented a mathematical model with a set of one-dimensional linear diffusion equations to simulate the transport problems of carbon-dioxide, chloride and sulphate ions in concrete.

Isgor and Razaqpur [19] proposed a nonlinear finite element approach for modelling coupled heat transfer, moisture transport and carbonation processes in concrete for tracing the spatial and temporal advancement of the carbonation front in concrete structures with and without cracks. The numerical results were compared with available experimental data. Kumazaki [20] presented a mathematical model of carbon-dioxide transport in concrete carbonation process. The model was described by using a parabolic type equation with a nonlinear perturbation such that a coefficient of the time derivative contains a non-local term depending on the unknown function itself. Zhang [21] developed a mathematical model of carbonation process in porous concrete materials. The model was solved numerically using uncoupled finite volume method. Numerical simulations under normal and accelerated carbonation conditions were presented. Zhu et al. [22] proposed a comprehensive model to simulate the transports of carbon-dioxide, chloride ions, heat and moisture in concrete. The model was validated using several sets of experimental data.

The above survey of literature shows that many mathematical models have been developed to describe the carbonation phenomena in concrete. However, most of existing models are difficult to use either because they require too many input data or because they were developed for some specific application cases. In this paper a mathematical model describing the diffusion of carbon-dioxide in concrete with considering the effect of concrete carbonation is developed. The diffusion model is established using Fick's first law, whereas the effect of concrete carbonation on carbon-dioxide diffusion is modelled by using a sink term added in the diffusion equation. The present diffusion model is simplified to the diffusion problem with a moving boundary representing the diffusion front or the carbonation depth when the

carbonation reaction is much faster than the diffusion process. An analytical solution is also derived from the diffusion problem of moving boundary for calculating corresponding carbonation depth.

2. Modelling of carbon-dioxide diffusion in concrete with general carbonation reaction

Concrete carbonation commonly takes place after the atmospheric carbon-dioxide, CO_2, diffuses into concrete from the air through concrete gaseous phase. The chemical reactions occurring during concrete carbonation can be broken down into two stages. One is the dissolving of CO_2 in pore solution and the other is the reaction of the dissolved CO_2 with the hydration products (mainly calcium ions) within the cement phase of concrete. The detailed description of the reactions for concrete carbonation can be found in the work of Bary and Sellier [23]. Nevertheless, the following represents the main reaction taking place during the concrete carbonation [24],

$$Ca(OH)_2(\mathrm{s} \rightarrow \mathrm{aq}) + CO_2(\mathrm{g} \rightarrow \mathrm{aq}) \rightarrow CaCO_3(\mathrm{aq} \rightarrow \mathrm{s}) + H_2O\ (\mathrm{aq}) \quad (1)$$

where the dissolved $Ca(OH)_2$ in pore solution will quickly decompose into calcium and hydroxide ions. Thus, Eq.(1) can be also expressed as follows,

$$Ca^{2+}(\mathrm{aq}) + 2OH^{-}(\mathrm{aq}) + CO_2(\mathrm{aq}) \rightarrow CaCO_3(\mathrm{s}) + H_2O(\mathrm{aq}) \quad (2)$$

where “g”, “aq” and “s” are the abbreviation of gaseous, aqueous and solid phase, respectively.

The transport of CO_2 in concrete gaseous phase can be described by using Fick laws with considering the consumption of CO_2 due to carbonation as follows [25,26,27],

$$\frac{\partial C}{\partial t} = \nabla(D\nabla C) - Q_{CO2} \quad (3)$$

where C in kg/m^3 is the content of CO_2 freely diffusing in concrete gaseous phase, t in s is the time, D in m^2/s is the diffusion coefficient of CO_2 in concrete gaseous phase, and Q_{CO2} in kg/(s-m^3) is the sink term representing the consumption rate of CO_2 due to carbonation, which can be approximated as follows [21,28],

$$Q_{CO2} = \frac{\partial S}{\partial t} = k_t(S_a - S) \tag{4}$$

where S in kg/m^3 is the content of CO_2 consumed due to carbonation, k_t in s^{-1} is the reaction rate constant, and S_a in kg/m^3 is the available content of CO_2 that can be consumed at a given condition.

Assume that the calcium ions in the pore solution are initially uniformly distributed and the process of their transport in the pore solution is much slower than that of their reaction taking place during carbonation. In this case the carbonation rate will be mainly controlled by calcium ions and S_a can be assumed to have the following expression,

$$S_a = S_{max}\left[1 - \exp\left(-\frac{k_a C}{C_s}\right)\right] \tag{5}$$

where S_{max} in kg/m^3 is the maximum content of CO_2 that can be consumed in carbonation, C_s in kg/m^3 is the content of CO_2 on the exposed surface (i.e. the content of CO_2 in environment where the concrete is exposed), and k_a is a dimensionless constant, which is used to reflect the effect of CO_2 concentration in gaseous phase on the relationship between S_a and S_{max}. The reaction rate constant k_t and dimensionless constant k_a can be determined using experimental data obtained from concrete carbonation tests. In general, they would be dependent on the temperature and relative humidity of the environment surrounding the concrete and the properties of concrete raw materials. Fig.1 graphically shows the relationship between S_a and C. It can be seen from the figure that when $k_a \to \infty$, $S_a = S_{max}$; indicating that S_a is a constant

except at the point of C=0. Substituting Eq.(5) into (3) and (4), it yields,

$$\frac{\partial C}{\partial t} = \nabla(D\nabla C) - k_t S_{max}\left[1 - \exp\left(-\frac{k_a C}{C_s}\right) - \frac{S}{S_{max}}\right] \quad (6)$$

$$\frac{\partial S}{\partial t} = k_t S_{max}\left[1 - \exp\left(-\frac{k_a C}{C_s}\right) - \frac{S}{S_{max}}\right] \quad (7)$$

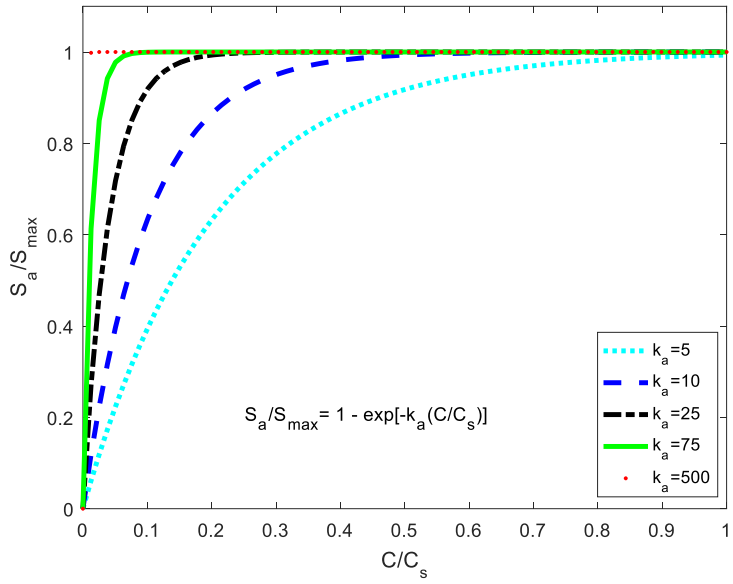

Fig. 1. Relationship between S_a and C.

Eqs.(6) and (7) are the governing equations which can be used to determine the content of CO_2 diffusing in concrete gaseous phase and the content of CO_2 consumed during concrete carbonation. The corresponding initial and boundary conditions of $C(t,x)$ and $S(t,x)$ can be expressed as follows,

Initial conditions:

$$C(0,x) = 0 \quad (8)$$

$$S(0,x) = 0 \quad (9)$$

Boundary conditions:

$$C(t,0) = C_s, \quad C(t,\infty) = 0 \quad (10)$$

$$S(t,0) = S_{max}, \quad S(t,\infty) = 0 \tag{11}$$

Eqs.(6)-(11) completely describe the transport problem of carbon-dioxide in concrete with taking into account the effect of concrete carbonation. Eqs.(6)-(11) can be solved using numerical methods such as the finite difference method [26,27]. Fig.2 shows the distribution profiles of $C(t,x)$ and $S(t,x)$ at a given time for various different values of k_a and k_t, obtained from the numerical solutions. It can be seen from the figure that the distribution pattern of the concentration profile of CO_2 is more sensitive to the profile constant k_a describing S_a than to the reaction rate constant k_t. An important feature that can be observed is the idealized situation of $k_a \to \infty$ and $k_t/D \to \infty$ (red line shown in Fig.2) in which the diffusion of CO_2 accompanied by the instantaneous and irreversible consumption of a limited amount of the diffusing CO_2, leading to a sharp front of the consumed CO_2. In front of the advancing boundary the content of the freely diffusing CO_2 is zero, while behind it the content of the consumed CO_2 is complete. This problem is similar to the heat flow in a medium which undergoes a phase change at some fixed temperature, accompanied by the absorption or liberation of latent heat.

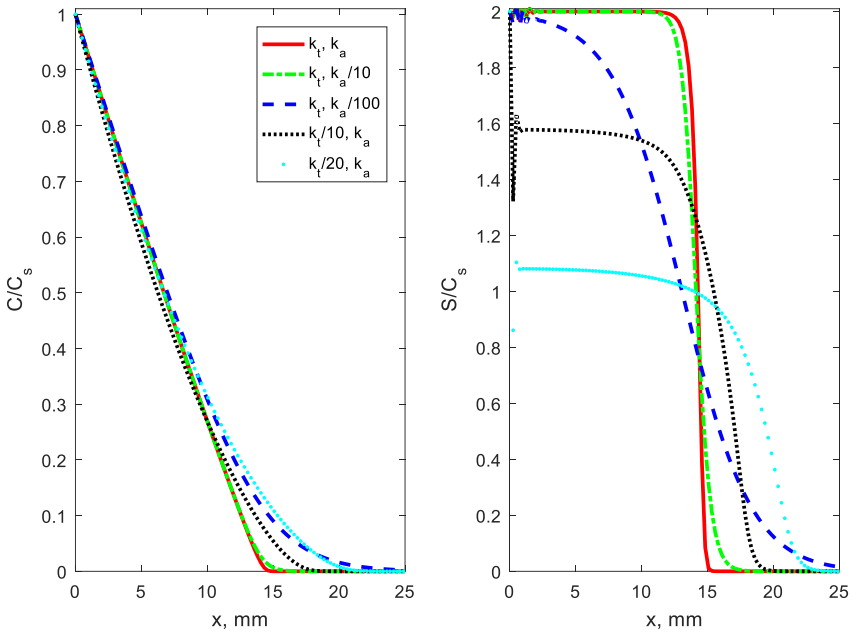

158

159 (a) (b)

160 **Fig. 2.** Effects of k_t and k_a on the distribution profiles of (a) CO_2 in gaseous phase and (b)

161 consumed CO_2 due to carbonation (k_t=10^{-6} s^{-1}, k_a=500, D=1.5x10^{-11} m^2/s, S_{max}/C_s=2,

162 $\sqrt{(Dt)}$=15.3 mm).

163

164 It is also observed from Fig.2 that when k_t or k_a is small the front of the consumed CO_2

165 profile is not steeply straight but slowly decreases with increased distance, indicating that the

166 carbonation reactions still take place in part of the carbonated zone. The transport of CO_2 in

167 the carbonated zone thus can be divided into two sub-zones. One is the fully carbonated zone

168 in which the transport of CO_2 is governed by diffusion only; the other is the partially carbonated

169 zone in which the transport of CO_2 is governed not only by diffusion but also by carbonation.

170 As an example, Fig.3a shows the profiles of the consumed CO_2 at various different times

171 obtained from the present model. It is obvious from the figure that the carbonation reactions

172 still take place in the zone behind the carbonation front. The carbonation depth for a given time

173 can be obtained from the carbonation front. By identifying the carbonation fronts from the
174 profiles of consumed CO_2 obtained at various different times we can find the relationship
175 between the carbonation depth and exposure time, which is plotted in Fig.3b. To demonstrate
176 the present model, experimental data [1] obtained from accelerated carbonation tests are also
177 superimposed in the figure. The experimental work was carried out inside a test chamber with
178 CO_2 concentration about 50 percent. The specimens tested were mortars with high water-to-
179 cement ratio 0.8. The parametric values used in the simulation are chosen to match the
180 experimental data. The results shown herein illustrate that the relationship between the
181 carbonation depth and exposure time may not necessarily follow the time square root relation
182 when the carbonation reactions are not faster than the diffusion speed of CO_2 in the gaseous
183 phase. Note that, in many carbonation tests of concrete the carbonation depth is determined by
184 using the phenolphthalein indicator solution [25,28], which is a colourless acid/base indicator
185 and can turn purple when its pH value exceeds 9. However, this test does not give the depth of
186 maximum ingress of CO_2 (i.e., the front point of partially carbonated zone) since the CO_2 in
187 the partially carbonated zone may cause a decrease in the pH-value beyond the carbonation
188 depth indicated by the phenolphtalein spray test, but their pH value may still be over 9.
189

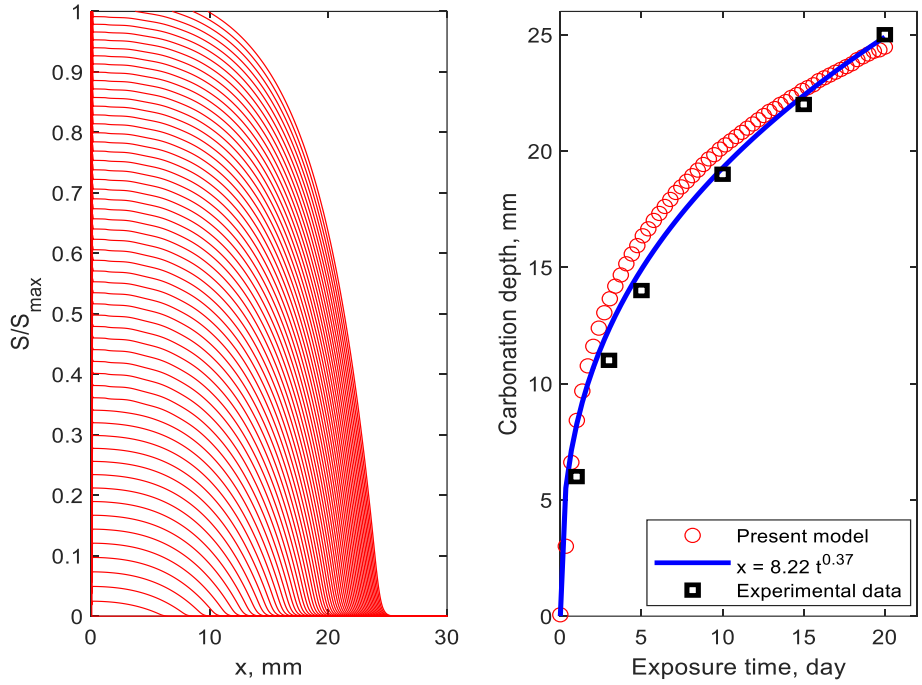

(a) (b)

Fig. 3. (a) Profiles of consumed CO_2 at various different times. (b) Variation of carbonation depth with exposure time (k_t=4.25x10^{-7} s^{-1}, k_a=5000, D=6.0x10^{-11} m^2/s).

In most cases, however, the chemical reaction between the carbonate ions and the calcium ions in pore solution is much quicker than the diffusion of the CO_2 in the gaseous phase. Hence, the reaction can be assumed to take place only at the diffusion front, whereas the transport of CO_2 can be assumed to take place only in the gaseous phase of the carbonated concrete. The consumption of CO_2 in the diffusion front can be assumed to be controlled by the availability of the $Ca(OH)_2$ or calcium ions in the pore solution. Under these assumptions, both k_a and k_t/D can be assumed to be infinitely large and the corresponding diffusion model described above requires only three constants D, C_s and S_{max}; each has a clearly physical meaning. Physically, this may represent the natural carbonation case where CO_2 ingress is relatively slow, whereas

the carbonation reaction is relatively fast.

Note that there is some numerical difficulty for solving Eqs.(6)-(11) when $k_a \to \infty$ and $k_t/D \to \infty$. Nevertheless, numerically, one can employ any large numbers for k_a and k_t/D to achieve the approximate solutions of the idealised case of $k_a \to \infty$ and $k_t/D \to \infty$. As a numerical example, Fig.4 shows the distribution profiles of $C(t,x)$ and $S(t,x)$ obtained at three different times that correspond to the parametric values $\sqrt{Dt}$ =8.82 mm, 12.5 mm and 15.3 mm, respectively, when k_a=500 and k_t=1.0x10^{-6} s^{-1} ($\sqrt{k_t/D}$=211 m^{-1}) are employed. It is clear from the figure that the distribution profiles of $S(t,x)$ terminate nearly abruptly in all of the three times. The infinite gradient at the diffusion front leads to some oscillations in the start point of the profiles. This implies that if care was not taken in the selection of spatial and time intervals, the numerical solution may become inaccurate.

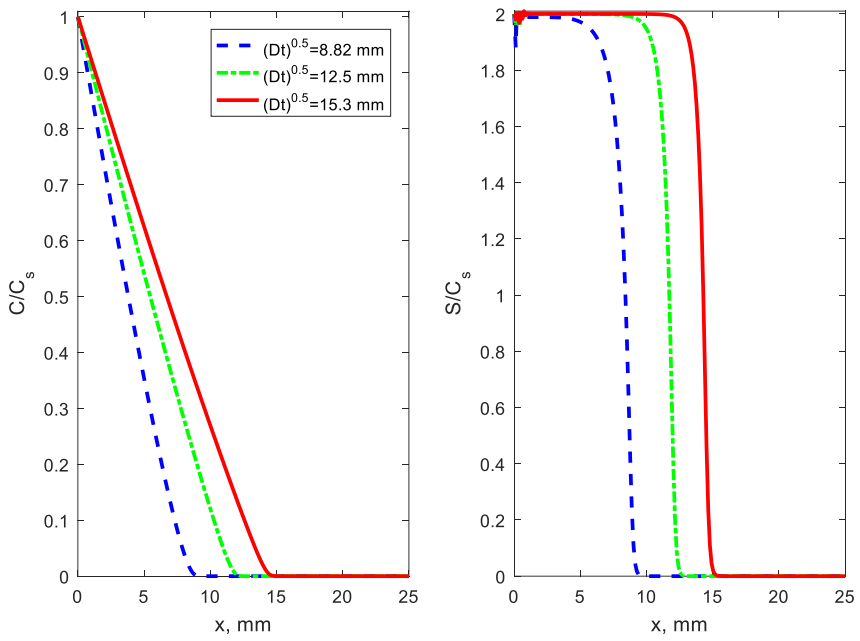

(a) (b)

Fig. 4. Concentration profiles of (a) CO_2 in gaseous phase and (b) consumed CO_2 at different

219 times (k_t=10^{-6} s^{-1}, k_a=500, D=1.5x10^{-11} m^2/s, S_{max}/C_s=2).

220

221 **3. Modelling of carbon-dioxide diffusion in concrete with fast carbonation reaction**

222 For the case where the carbonation reactions are fast while the carbon-dioxide diffusion
223 is slow the transport model described in Section 2 can be simplified by assuming $k_a \to \infty$ and
224 $k_t/D \to \infty$. To avoid the numerical difficulty when solving the idealised case of $k_a \to \infty$ and
225 $k_t/D \to \infty$, the transport problem of carbon-dioxide in concrete with taking into account the
226 effect of concrete carbonation described in Section 2 is now treated as the diffusion problem of
227 particles in which part of particles are trapped in stationary holes. By considering the mass
228 change of the total CO_2 in a unit volume of concrete in a time interval dt, the following mass
229 conservation equation can be established,

230 $$\frac{\partial C_T}{\partial t} = \nabla(D\nabla C) \tag{12}$$

231 where C_T=C+S in kg/m^3 is the total content of CO_2 in concrete. The right-hand-side of Eq.(12)
232 is the flux gradient based on the Fick's first law, in which C in kg/m^3 is the content of CO_2
233 freely diffusing in the gaseous phase of carbonated concrete. The initial and boundary
234 conditions of $C_T(t,x)$ can be expressed as follows,

235 $$C_T(0,x) = 0 \tag{13}$$

236 $$C_T(t,0) = C_s + S_{max}, \quad C_T(t,\infty) = 0 \tag{14}$$

237 When solving Eqs.(12)-(14) for C_T one has to know the content of CO_2 in concrete gaseous
238 phase, which is the function of C_T and S_{max} and can be expressed as follows,

239 $$C(t,x) = \begin{cases} C_T(t,x) - S_{max} & C_T(t,x) > S_{max} \\ 0 & C_T(t,x) \le S_{max} \end{cases} \tag{15}$$

240 Note that, in the region of $C_T(t,x)>S_{max}$ all holes are completely filled, whereas in the
241 region of $C_T(t,x)<S_{max}$ the holes are not completely filled and therefore $C(t,x)=0$.
242 Eqs.(12)-(15) can be used for solving for $C_T(t,x)$ and thus $C(t,x)$ can be obtained.
243 Compared to the model described in Section 2, the model presented herein by Eqs.(12)-(15) is
244 much simple, clear, concise and easy to solve. As a numerical example, Fig.5 shows the
245 distribution profiles of $C(t,x)$ and $S(t,x)$ at three different times obtained from the present model.
246 For the purpose of comparison, the results obtained from the model described in Section 2 are
247 also superimposed in the figure. It can be observed from the figure that there is almost no
248 difference in the results of $C(t,x)$ obtained from the two models. There is only a small difference
249 in the results of $S(t,x)$ at the diffusion front obtained from the two models. To examine the
250 spatial-time relationship, Fig.6 replots the three profiles of $C_T(t,x)$ shown in Fig.5 but using a
251 combined spatial and time coordinate, $x/\sqrt{(Dt)}$. It can be seen from the plot that when the
252 combined coordinate is used the profiles at three different times are merged together, indicating
253 that the diffusion depth of CO_2 is proportional to the square root of the diffusing time.
254

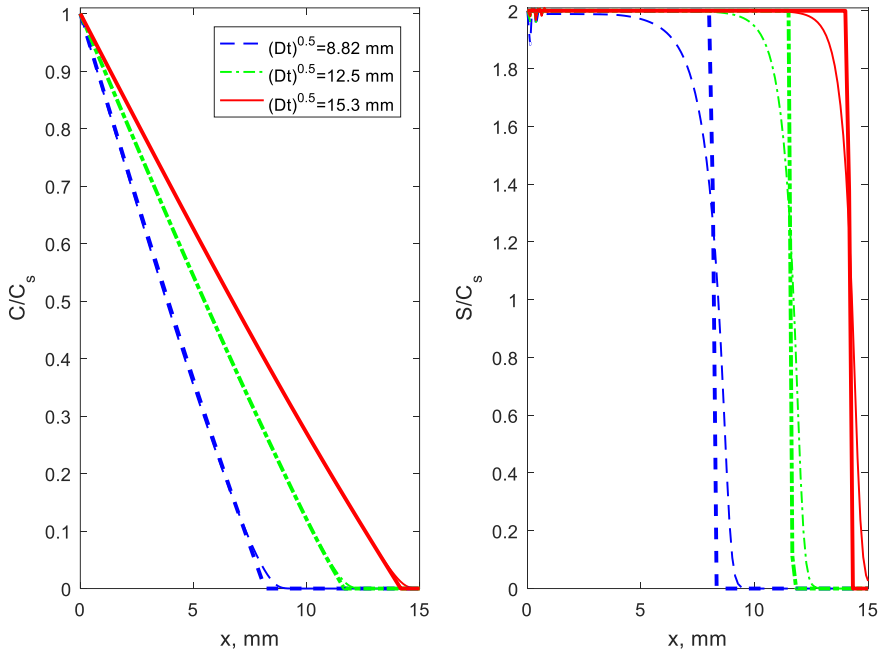

(a) (b)

Fig. 5. Comparisons of (a) CO_2 profiles and (b) consumed CO_2 profiles between general and fast carbonation reaction models (thin and thick lines represent the results of general and fast reaction models, respectively, D=1.5x10^{-11} m^2/s).

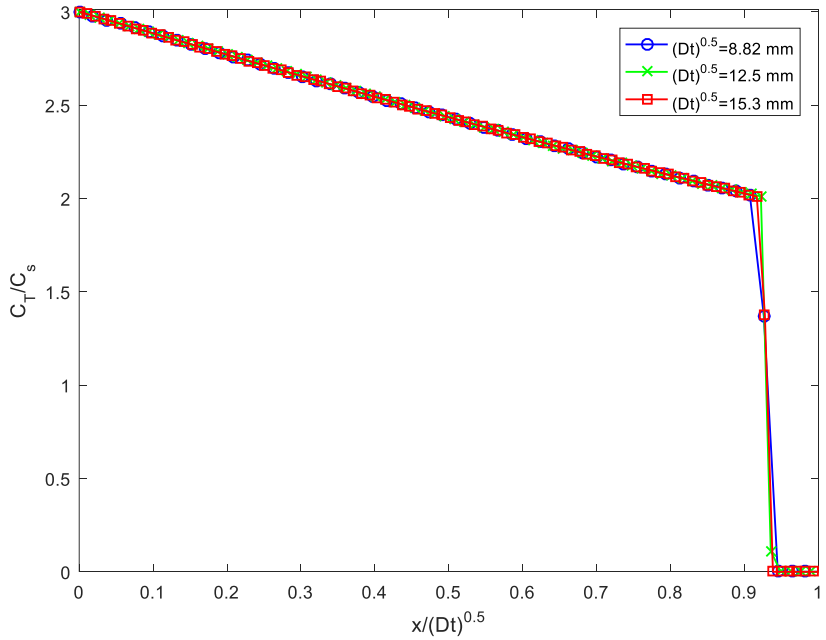

Fig. 6. Concentration profiles of total CO_2 at three different times plotted against combined

spatial and time coordinate (D=1.5x10^{-11} m^2/s).

4. Modelling of carbon-dioxide diffusion in concrete with moving boundary

The mass conservation equation (12) can be applied to any point in the domain ($0<x<\infty$). However, if it is applied only to the domain ($0<x<\xi$) where ξ is the diffusion front, then $\frac{\partial C_T}{\partial t} = \frac{\partial C}{\partial t}$ since S=S_{max} is a constant in the domain ($0<x<\xi$). Thus, Eq.(12) can be further simplified to Eq.(16),

$$\frac{\partial C}{\partial t} = \nabla(D\nabla C) \qquad 0 < x < \xi \qquad (16)$$

The initial and boundary conditions of $C(t,x)$ can be expressed as follows,

$$C(0,x) = 0 \qquad (17)$$

$$C(t,0) = C_s, \;\; C(t,\xi) = 0 \qquad (18)$$

Note that ξ is the function of time, which moves forward when time increases. Thus Eqs.(16)-(18) represents the diffusion problem with moving boundary. As it is demonstrated in Section 3, the depth of the diffusion front is proportional to square root of the diffusing time. Thus, the following expression can be assumed for $\xi(t)$,

$$\xi(t) = k_\xi\sqrt{Dt} \qquad (19)$$

where k_ξ is a constant to be determined. The solution of Eq.(16) with the initial and boundary conditions defined by Eqs.(17) and (18) can be expressed as follows,

$$C(t,x) = C_s\left(1 - \frac{erf\left(\frac{x}{2\sqrt{Dt}}\right)}{erf\left(\frac{k_\xi}{2}\right)}\right) \qquad 0 \le x \le \xi \qquad (20)$$

where $erf(\cdot)$ is the error function. It is obvious from Eq.(20) that if k_ξ is known then the solution (20) for $C(t,x)$ is completely defined. In order to determine k_ξ an additional mass conservation

equation need to be established at the point of the diffusion front, which can be expressed as follows,

$$-D\frac{\partial C}{\partial x} = S_{max}\frac{d\xi}{dt} \qquad \text{for } x = \xi \qquad (21)$$

Physically, the left-hand-side of Eq.(21) represents the diffusion flux from the diffusion zone into the zone ahead of the diffusion front; whereas the right-hand-side of Eq.(21) represents the flux required in order that the diffusion front can advance by a distance of $d\xi$ in the time interval of dt. Substituting Eqs.(19) and (20) into (21), it yields,

$$\frac{k_\xi}{2} erf\left(\frac{k_\xi}{2}\right) exp\left(\frac{k_\xi^2}{4}\right) = \frac{C_s}{\sqrt{\pi} S_{max}} \qquad (22)$$

Eq.(22) is a nonlinear algebraic equation about k_ξ, which can be used to determine k_ξ for a given ratio of C_s/S_{max}. After k_ξ is determined it can be substituted into Eq.(19) for calculating the depth of diffusion front $\xi(t)$ and Eq.(20) for calculating the profile $C(t,x)$ of CO_2. Fig.7 graphically shows the relationship between k_ξ and C_s/S_{max}. It can be seen from the figure that k_ξ increases with C_s/S_{max}; initially very quick but it becomes slow afterwards. It is clear from Eq.(19) that the influence of C_s/S_{max} on $\xi(t)$ is the same as that it does on k_ξ. To demonstrate the analytical solutions presented by Eqs.(19) and (20), Fig.8 provides a comparison between the analytical solution given by Eqs.(19)-(20) and the numerical solutions given by Eqs.(12)-(15) for the concentration distribution profile of freely diffusing CO_2. As it is to be expected, there is no difference between the analytical and numerical solutions.

Of a particular interest is the case where $C_s/S_{max} \ll 1$ and/or $k_\xi \ll 1$, for which case the following approximation can be taken mathematically,

$$\frac{k_\xi}{2} erf\left(\frac{k_\xi}{2}\right) exp\left(\frac{k_\xi^2}{4}\right) \approx \frac{k_\xi^2}{2\sqrt{\pi}} \qquad (23)$$

Hence, Eq.(22) can be simplified as follows,

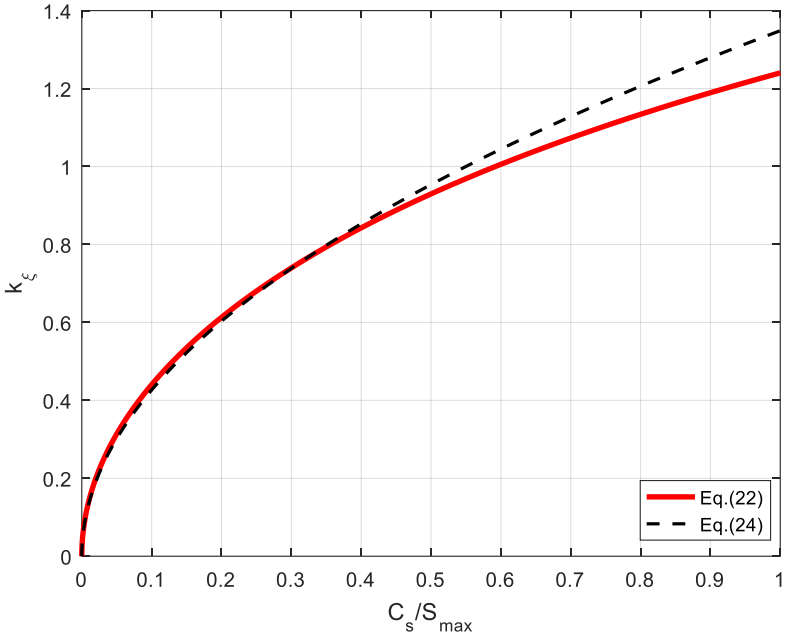

Fig. 7. Variation of k_ξ with C_s/S_{max}.

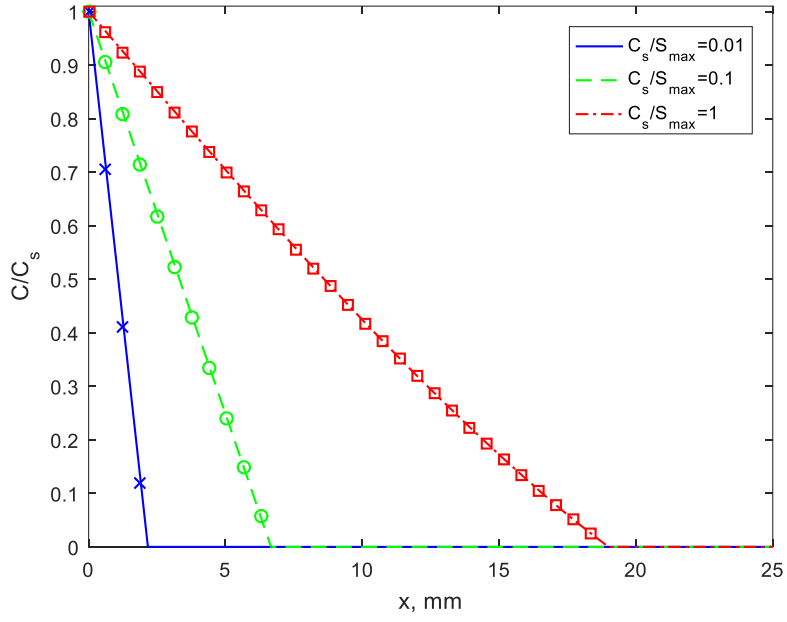

Fig. 8. Effect of C_s/S_{max} on CO_2 profiles at time $\sqrt{(Dt)}$=15.3 mm (lines are analytical solution given by Eqs.(19)-(20) and symbol points are numerical solutions given by Eqs.(12)-(15)).

$$k_\xi = \sqrt{\frac{2C_s}{S_{max}}} \tag{24}$$

The corresponding diffusion front $\xi(t)$ can be simplified as follows,

$$\xi(t) = \sqrt{\frac{2C_S Dt}{S_{max}}} \quad (25)$$

Eq.(25) is identical to that proposed by Papadakis et al. [1], Houst and Wittmann [29], Hyvert et al. [30], and Klopfer [31]. Experimental validation of Eq.(25) has been reported in literature, for example, [1,29,30,31,32], and thus is not provided herein. However, it is obvious from the above derivation that Eq.(25) is only limited to the case where the surface content of CO_2 is much lower than the consumed content of CO_2 in carbonation; otherwise one has to use more accurate equation, Eq.(22), instead of its simplified form, Eq.(24), to calculate the carbonation depth. Fig.7 shows the difference between k_ξ calculated from Eq.(22) and that calculated from Eq.(24), from which one can clearly see the difference between them can be ignored for C_s/S_{max}<0.5. Compared with existing work, not only can the present analytical solution be used to predict the carbonation depth but also to estimate the profile of CO_2 in the carbonated concrete.

CO_2 level in the atmosphere is normally expressed as parts per million or ppm. It was reported that the CO_2 level increases in recent years and was at 391 ppm in March of 2011, which is 0.0391% of the atmosphere. The air density can be approximately taken as 1.225 kg/m^3. This gives the content of CO_2 in air is about 0.479 g/m^3. The maximum amount of CO_2 that can be consumed in concrete carbonation can be estimated as follows [33],

$$S_{max} = 0.75 CaO Cem \frac{M_{CO2}}{M_{CaO}} = 0.377 Cem \quad (26)$$

where CaO (≈0.64) is the amount of calcium oxide per weight of cement, Cem is the content of cement used in concrete, M_{CO2}=44 g/mol and M_{CaO}=56 g/mol are the molar weight of CO_2 and CaO, respectively. For normal Portland cement concrete Cem is about 350 kg/m^3. This gives S_{max}=132 kg/m^3 and thus C_s/S_{max}=0.36x10^{-5}, which indicates that Eq.(24) can be safely

used for most natural carbonation cases unless for specific laboratory tests where the concentration of CO_2 used is much higher and the tested concrete is with supplementary cementitious materials (SCMs) which may reduce the content of the cement used in concrete.

5. Conclusions

In this paper we have presented the mathematical models to describe the diffusion of carbon-dioxide in concrete with considering the effect of concrete carbonation. Three models have been discussed, namely the diffusion model with general carbonation reaction, the diffusion model with fast carbonation reaction, and the diffusion model with moving boundary. Numerical solutions have been provided for the first two models, whereas analytical solution has been derived for the third model. Comparisons between the three models have been also provided, which illustrates their advantages and disadvantages. From the present study the following conclusions can be drawn:

- In the diffusion model with general carbonation reaction the distribution pattern of the concentration profile of CO_2 is more sensitive to the profile constant k_a describing S_a than to the reaction rate constant k_t.
- It is more convenient to use the total concentration of CO_2 to model the diffusion of CO_2 in concrete with fast carbonation reaction, which avoids the difficulty of moving boundary. The diffusion front obtained from the numerical model for the diffusion model with fast carbonation reaction represents the carbonation depth.
- The analytical solution presented for the diffusion model with moving boundary can be

directly used to examine the effects of diffusion coefficient of CO_2 in carbonated concrete, diffusing time, and the ratio of C_s-to-S_{max} on the depth of concrete carbonation.

- It is demonstrated from the present analytical solution that the square root dependence of carbonation depth on C_s/S_{max} provided in many existing studies is appropriate only for the case where C_s/S_{max} is very small; otherwise more accurate nonlinear equation, Eq.(22), instead of its simplified form, Eq.(24), should be used for calculating the carbonation depth.

Acknowledgements

The authors would like to acknowledge the financial support received from the National Natural Science Foundation of China (Grant No. 51520105012). Part of the present work was also supported by the European Commission Research Executive Agency via a Marie Skłodowska-Curie Research and Innovation Staff Exchange project (H2020-MSCA-RISE-2017, TRAC-777823).

References

[1] V.G. Papadakis, C.G. Vayena, M.N. Fardis, Fundamental modelling and experimental investigation of concrete carbonation. ACI Materials Journal 88(4) (1991) 363-373.

[2] A.V. Saettaa, R.V. Vitaliani, Experimental investigation and numerical modeling of carbonation process in reinforced concrete structures, Part I: theoretical formulation. Cement and Concrete Research 34(4) (2004) 571–579.

[3] A.W. Islam, T.A. Meckel, A.Y. Sun, P.G. Krishnamurthy, Numerical experiments of density driven CO_2 saturated brine migration in heterogeneous two-dimensional geologic fabric materials. Int. Comm. Heat Mass Transfer 71 (2016) 148-156.

[4] V.T. Ngala, C.L. Page, Effects of carbonation on pore structure and diffusion properties of hydrated cement pastes. Cement and Concrete Research 27(7) (1997) 995–1007.

[5] J. Geng, D. Easterbrook, Q.F. Liu, L.Y. Li, Effect of carbonation on releaseof bound chlorides in chloride-contaminated concrete. Magazine of Concrete Research 68(7) (2016) 353-363.

[6] M.E. Aguilera, A.L. de Ramos, Effect of CO_2 diffusion on wettability for hydrocarbon-water-CO_2 systems in capillaries. Int. Comm. Heat Mass Transfer 31(8) (2004) 1115-1122.

[7] A. Ibrahim, D. Lemonnier, Numerical study of coupled double-diffusive natural convection and radiation in a square cavity filled with A N_2–CO_2 mixture. Int. Comm. Heat Mass Transfer 36(3) (2009) 197-202.

[8] H.Z. Yuan, X.R. Zhang, Numerical simulation with adaptive finite element methods for CO_2 storage in saline aquifers. Int. Comm. Heat Mass Transfer 45 (2013) 55-63.

[9] R.K. Dhir, M.R. Jones, M.J. McCarthy, PFA concrete: Chloride ingress and corrosion in carbonated cover. Proceedings of the Institution of Civil Engineers: Structures and Buildings 99(2) (1993) 167-172.

[10] C. Yuan, D. Niu, D. Luo, Effect of carbonation on chloride diffusion in fly ash concrete. Disaster Advances 5(4) (2012) 433-436.

[11] W.P.S. Dias, Reduction of concrete sorptivity with age through carbonation. Cement and

Concrete Research 30(8) (2000) 1255–1261.

[12] I.S. Yoon, O. Copuroglu, K.B. Park, Effect of global climate change on carbonation progress of concrete. Atmospheric Environment 41(34) (2007) 7274-7285.

[13] M.F. Montemor, A.M.P. Simoes, M.G.S. Ferreira, Chloride-induced corrosion on reinforcing steel: from the fundamentals to the monitoring techniques. Cement and Concrete Composites 25(4-5) (2003) 491-502.

[14] M. Jin, S. Gao, L. Jiang, H. Chu, M. Lu, F.F. Zhi, Degradation of concrete with addition of mineral admixture due to free chloride ion penetration under the effect of carbonation. Corrosion Science 138 (2018) 42-53.

[15] X.J. Zhu, G.S. Zi, W.W. Lee, S.Y. Kim, J.S. Kong, Probabilistic analysis of reinforcement corrosion due to the combined action of carbonation and chloride ingress in concrete. Construction and Building Materials 124 (2016) 667-680.

[16] A.V. Saetta, B.A. Schrefler, R.V. Vitaliani, 2-D model for carbonation and moisture/heat flow in porous materials. Cement and Concrete Research 25(8) (1995) 1703-1712.

[17] A. Steffens, D. Dinkler, H. Ahrens, Modeling carbonation for corrosion risk prediction of concrete structures. Cement and Concrete Research 32(6) (2002) 935-941.

[18] M.T. Liang, S.M. Lin, Modeling the transport of multiple corrosive chemicals in concrete structures: Synergetic effect study. Cement and Concrete Research 33(12) (2003) 1917-1924.

[19] O.B. Isgor, A.G. Razaqpur, Finite element modeling of coupled heat transfer, moisture transport and carbonation processes in concrete structures. Cement and Concrete Composites 26(1) (2004) 57-73.

419 [20] K. Kumazaki, A mathematical model of carbon dioxide transport in concrete carbonation
420 process. Discrete and Continuous Dynamical Systems (Series S) 7(1) (2014) 113-125.
421 [21] Q. Zhang, Mathematical modeling and numerical study of carbonation in porous concrete
422 materials. Applied Mathematics and Computation 281 (2016) 16-27.
423 [22] X.J. Zhu, G.S. Zi, Z.F. Cao, X.D. Cheng, Combined effect of carbonation and chloride
424 ingress in concrete. Construction and Building Materials 110 (2016) 369-380.
425 [23] B. Bary, A. Sellier, Coupled-carbon dioxide-calcium transfer model for carbonation of
426 concrete. Cement and Concrte Research 34(10) (2004) 1859-1872.
427 [24] M.A. Peter, A. Muntean, S.A. Meier, M. Böhm, Competition of several carbonation
428 reactions in concrete: A parametric study. Cement and Concrete Research 38(12) (2008)
429 1385-1393.
430 [25] M. Thiery, G. Villain, P. Dangla, G. Platret, Investigation of the carbonation front shape
431 on cementitious materials: Effects of the chemical kinetics. Cement and Concrete
432 Research 37(7) (2007) 1047-1058.
433 [26] M.B.A. Monsour, Travelling wave solutions of a nonlinear reaction–diffusion–chemotaxis
434 model for bacterial pattern formation. Applied Mathematical Modelling 32(2) (2008)
435 240–247.
436 [27] G. Carey, N. Fowkes, A. Staelens, A. Pardhanani, A class of coupled nonlinear reaction
437 diffusion models exhibiting fingering. J. Comput. Appl. Math. 166(1) (2004) 87–99.
438 [28] RILEM, CPC-18 measurement of hardened concrete carbonation depth. Materials and
439 Structures 21(6) (1988) 453–455.
440 [29] Y.F. Houst, F.H. Wittmann, Depth profiles of carbonates formed during natural carbonation.

441 Cement and Concrete Research 32(12) (2002) 1923–1930.
442 [30] N. Hyvert, A. Sellier, F. Duprat, P. Rougeau, P. Francisco, Dependency of C–S–H
443 carbonation rate on CO_2 pressure to explain transition from accelerated tests to natural
444 carbonation. Cement and Concrete Research 40(11) (2010) 1582–1589.
445 [31] H. Klopfer, The carbonation of external concrete and the control of it. Bautenschutz
446 Bausanier 1(3) (1978) 86-97.
447 [32] K. Sisomphon, L. Franke, Carbonation rates of concretes containing high volume of
448 pozzolanic materials. Cement and Concrete Research 37(12) (2007) 1647–1653.
449 [33] C. Pade, M. Guimaraes, The CO_2 uptake of concrete in a 100 year perspective. Cement
450 and Concrete Research 37(9) (2007) 1348-1356.